The free surface effect: Implications for amplitude-versus-offset inversion[1]

David W.S. Eaton

ABSTRACT

The magnitude and direction of P-wave particle displacement at the earth's surface differs from the particle displacement within the earth due to the interaction of the wavefield with the free surface. Synthetic models of a low impedance contrast gas sand are used to investigate the significance of the free surface effect in the context of AVO analysis. The gas sand is 15 m thick, and buried to a depth of 1500 m beneath a layer having a velocity that increases with depth in a linear fashion. Inversion of the synthetic data shows that the estimated Poisson's ratio of the gas sand can exhibit very significant error if the free surface effect is not accounted for. The magnitude of the error is largest for a high velocity near surface layer. This situation may occur either when bedrock is exposed at the surface or when the ground is frozen.

INTRODUCTION

Consider a plane P wave that impinges at nonnormal incidence against the free boundary of an isotropic elastic half space. At the moment the incident P wave strikes a position $\mathbf{X}_0$ on the boundary, a reflected P wave and a mode converted SV wave are generated (Figure 1). The net particle motion at $\mathbf{X}_0$ is the vector sum of the motions associated with the three waves, and in general is neither vertical nor parallel to the direction of the incident wave (Figure 1, inset). The magnitude and direction of the net displacement vector $\mathbf{u}_n$ is a function of the angle of incidence at the free surface and the elastic properties of the medium. The manner in which $\mathbf{u}_n$ differs from the incident particle displacement vector $\mathbf{u}_i^p$ is referred to herein as the "free surface effect".

For many years, the significance of abrupt changes in the Poisson's ratio of rock strata in the amplitude versus offset (AVO) relationship for reflected P waves has been recognized (Koefoed, 1955; Ostrander, 1984). In practice, an estimate of the Poisson's ratio of rock strata can be obtained by inversion of observed amplitude variations in CMP gathers (Yu, 1985). One method of implementing the inversion is by minimization of the squared difference between the results of forward modeling using the Zoeppritz equations and the observed data, after normalization by the amplitudes at zero offset. The accuracy of this method is contingent on both the degree to which the data acquisition and processing have preserved "true relative" amplitudes and the validity of the forward modeling process. In some cases, either the total particle displacement or vertical component of the emergent wavefield are calculated during forward modeling, rather than the actual vertical component of particle displacment at the free surface. The intent of this paper is to assess the magnitude of the inversion error that can result under these circumstances.

In order to study the free surface effect in the context of a realistic exploration scenario, a simple velocity/depth model representing a 15 m thick gas saturated

---

[1] Reprinted with the permission of the Journal of the Canadian Society of Exploration Geophysicists.

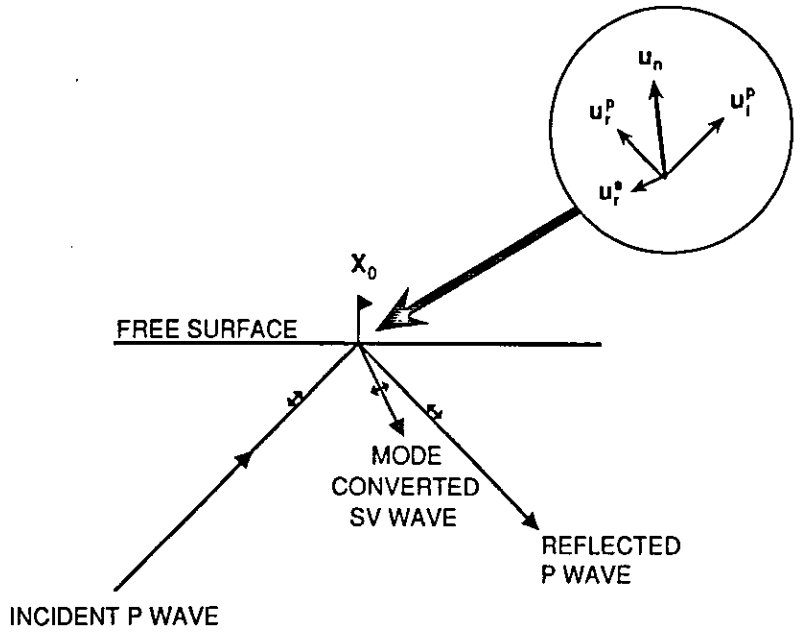

FIG. 1. When a P wave strikes the free surface, a reflected P wave and a mode converted SV wave are generated. The net particle motion at the free surface arises from the superposition of all three waves. Vector arrows in inset represent maximum particle displacement. $\mathbf{u}_i^p$ = incident P-wave displacment, $\mathbf{u}_r^p$ = reflected P-wave displacement, $\mathbf{u}_r^s$ = mode converted SV-wave displacement, $\mathbf{u}_n$ = net particle displacement.

sandstone reservoir buried beneath 1500 m of Cretaceous sediments was chosen (Table 1). Normal incidence reflections from this gas sand are relatively weak, but reflection strength increases rapidly with increasing incidence angle corresponding to sand Class 2 of Rutherford and Williams (1989). The velocity/depth relationship in the Cretaceous section is taken to be linear with depth (z)

$$\alpha(z) = \alpha_0 + \kappa_\alpha z \qquad (1)$$

with κ_α=0.25 (Jain, 1987). For a velocity function of this form, the raypaths are the arcs of circles centred at a height α_0/κ_α above the ground surface (Ostrander, 1984). Five earth models were created by allowing the near surface P-wave velocity to vary from 600 m/s - 3025 m/s and the near surface Poisson's ratios to vary from 0.4375 - 0.4000 (D.C. Lawton, *pers. comm.*). The thickness of the near surface layer is 10 m. Fifteen synthetic CMP gathers were ray- traced using these earth models, corresponding to the following particle displacement components:

- Total particle displacement due to the emergent wavefield only (series A);
- Vertical component of the emergent wavefield particle displacement (series B);
- Vertical component of particle displacement at the free surface (series C).

The displacement amplitude reflection coefficients were obtained using Young and Braile's (1976) program for solving Zeppritz's equations.

free surface boundary conditions. The receiver characteristics of a single vertical geophone are thus obtained by setting $|\mathbf{u}_i^p| = 1$ and solving for the vertical component of $\mathbf{u}_n$. The result can be expressed in terms of the near surface velocity ratio γ_{ns} (or alternatively the Poissons ratio of the near surface layer, σ_{ns}) and θ (Aki and Richards, 1980, p. 190; Dankbaar, 1985):

$$R_v^p(\theta,\gamma_{ns}) = \frac{2\cos\theta(2\gamma_{ns}^2\sin^2\theta-1)}{(1-2\gamma_{ns}^2\sin^2\theta)^2 + 4\gamma_{ns}^3\sin^2\theta\cos\theta(1-\gamma_{ns}^2\sin^2\theta)^{1/2}} \quad (2)$$

Note that this function is independent of the density of the near surface layer. Figure 2 shows a graph of R_v^p vs. θ for various values of σ_{ns}. In Figure 2, models 1 and 5 (see Table 1) represent the extremes of Poisson's ratio considered in the synthetic examples below. Also shown are curves for the theoretical Poisson's ratio limits of σ_{ns}=0 and 0.5; however, curves corresponding to intermediate values of Poisson's ratio do not necessarily lie between these two limiting cases. The graph indicates that the single vertical geophone receiving characteristics are only weakly dependent on σ_{ns} within a realistic range of values, and are primarily controlled by the angle of incidence at the surface, θ. For a given velocity/depth model, θ is governed primarily by the velocity in the near surface layer.

Angle of incidence at the free surface

Figure 3 shows the angle of incidence at the surface from the top of the gas sand vs. offset for models 1, 3 and 5 corresponding to near surface P-wave velocities of 600, 1800 and 3025 m/s respectively. Comparison with Figure 2 reveals that α_{ns} exerts a strong influence on the magnitude of the free surface effect. The presence of a low velocity weathered layer causes the raypaths to refract into near vertical incidence for which $R_v^p \approx -2$.

SYNTHETIC EXAMPLES

Synthetic 40-fold NMO corrected CMP gathers corresponding to near surface model 5 are plotted with true relative amplitudes in Figure 4. Model 5A was constructed by convolving the calculated reflection coefficients (Young and Braile, 1976) from the top and bottom of the gas sand with a 20 ms zero phase Ricker wavelet. Model 5B was created using the vertical component of the total displacement amplitudes in Model 5A. Model 5C represents the actual vertical component of displacement at the free surface. Geophone array effects, spherical divergence, NMO stretch and source-related effects have been ignored in this example. However, transmission losses and thin bed tuning have been accounted for. Note that models 5B and 5C are reversed in polarity relative to model 5A, and model 5C is approximately twice the amplitude of the other two.

An amplitude plot for the previous synthetic gathers is shown in Figure 5a. The values plotted are the RMS amplitude of the entire trace. RMS amplitude information was found to be considerably more robust for this type of analysis than simply picking peak event amplitudes from the trace (in practice, the RMS amplitude within a short time window containing the event of interest would be most useful). Figure 5b shows the AVO curve for models 1C, 3C and 5C, showing

Layer No	Name	Thickness (m)	α_o (m/s)	κ_α (s^{-1})	β_o (m/s)	κ_β (s^{-1})	ρ ($10^3 kg/m^3$)	σ
1	Upper Cretaceous	1500	3025	0.25	1235	0.102	2.4	Variable
2	Gas sand	15	3200	0	2133	0	2.2	0.1
3	Lower Cretaceous	∞	3400	0	1388	0	2.4	0.4

Table 1. Layered earth parameters.

THEORY

Assumptions and Notation

Although some of the layer thicknesses for the earth models being considered are much smaller than the dominant wavelength within them, the validity of the high frequency optics (ray theory) approximation is assumed. Some justification for this assumption is provided by the results of Moczo *et al.* (1987). Throughout the discussion, the following notation is used:

α: P-wave velocity
β: S-wave velocity
γ: Velocity ratio β/α
σ: Poisson's ratio
θ: Angle of incidence at the free surface

Free surface receiver characteristics

Displacement at a free surface is subject to the boundary condition that components of the stress dyadic in the plane of the surface must vanish (Aki and Richards, 1980, p. 135). When this condition is satisfied, reflected downgoing P and SV waves are generated whose amplitudes can be determined by solving the

Model No.	α_m (m/s)	β_m (m/s)	σ_m
1	600	200	0.4375
2	1200	459	0.4143
3	1800	718	0.4054
4	2400	976	0.4009
5	3025	1235	0.4000

Table 2. Near surface layer permutation models.

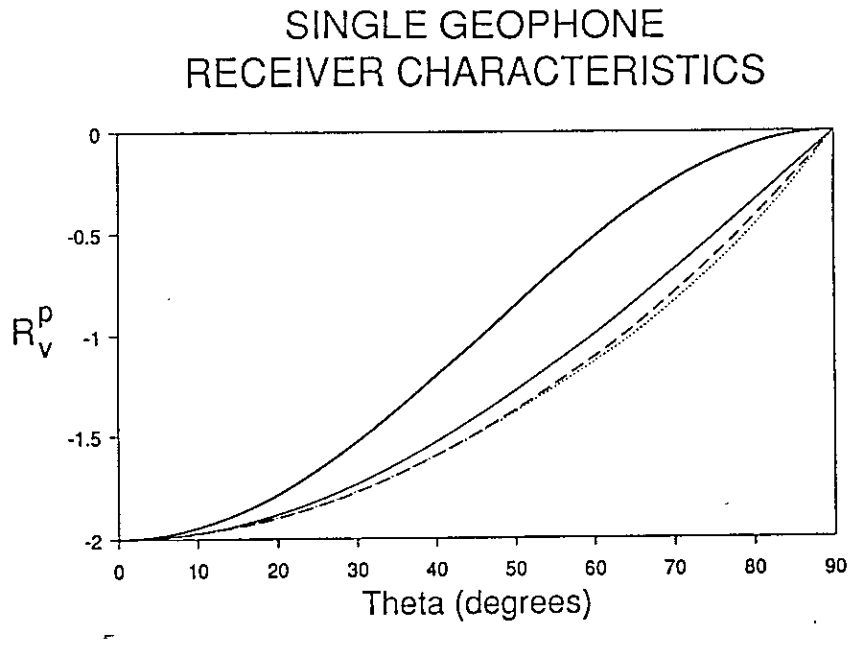

FIG. 2. Receiver characteristics for single vertical geophone (vertical component of $\mathbf{u}_n$) for various values of σ_{ns}. Models 1C (dashed line) and 5C (dotted line) represent the extreme values of σ_{ns} considered in the suite of synthetic models. Theoretical extreme cases are represented by $\sigma_{ns} = 0$ (thick line) and $\sigma_{ns} = 0.5$ (thin line). R_v^p is controlled primarily by the angle of incidence θ.

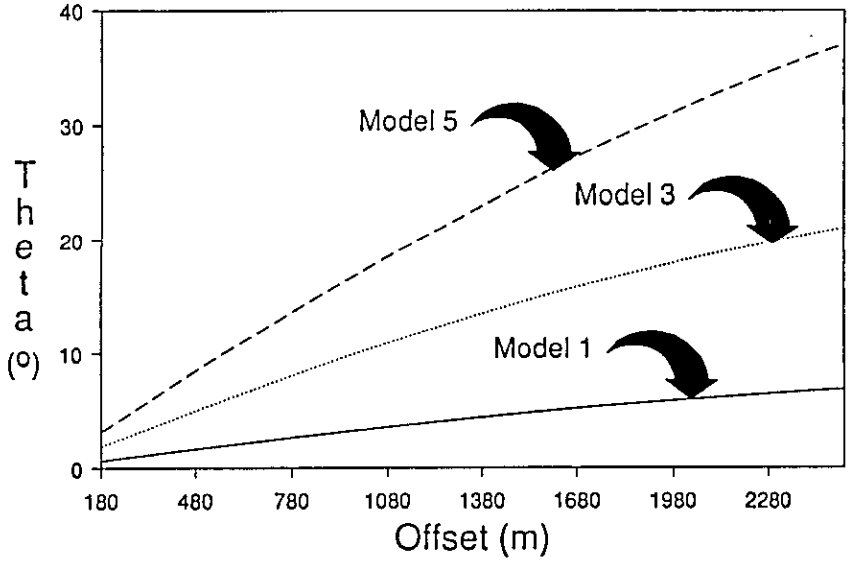

FIG. 3. Angle of incidence at the free surface versus offset for three of the synthetic models. θ is governed in these models by the near surface P-wave velocity.

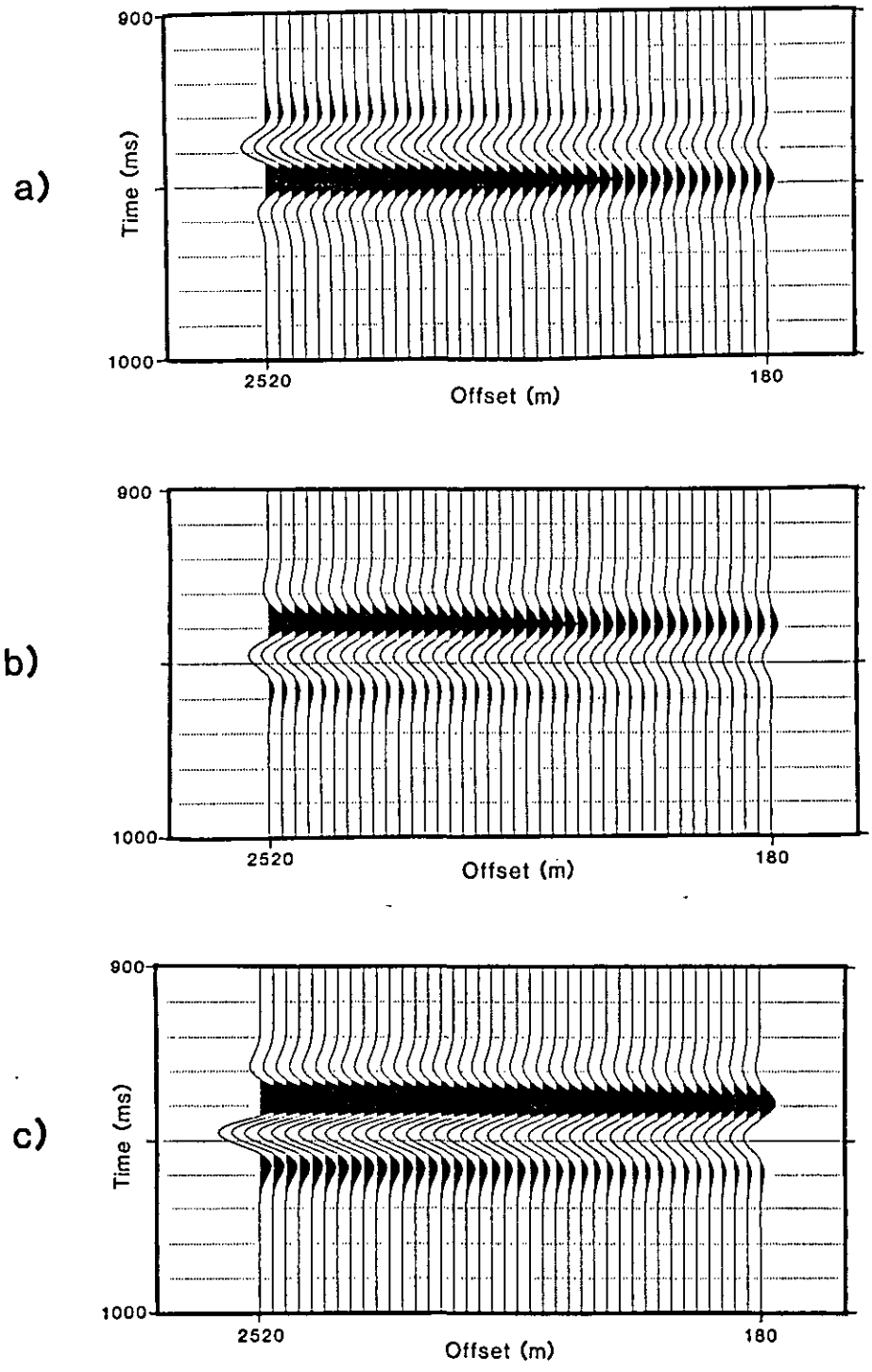

FIG. 4. (a) True amplitude display of a portion of NMO-corrected synthetic CMP gather for model 5A (total particle displacement for emergent ray only). Model parameters: trace spacing=60 m, fold=40, near offset=180 m, far offset=2520 m, sample rate=200 μs. (b) True amplitude display of a portion of NMO-corrected synthetic CMP gather for model 5B vertical component of particle displacement for emergent ray). (c) True amplitude display of a portion of NMO-corrected synthetic CMP gather for model 5C (vertical component of particle displacement at the free surface).

the direct effect that near surface velocity has on AVO. From these plots, the following observations can be made:

- for this velocity model, the free surface effect alters the magnitude but not the sign of the amplitude versus offset gradient;
- the significance of the free surface effect increases with near surface velocity.

In the reverse situation to the examples considered here (amplitude decreases with offset), the free surface effect will cause the decrease to be more dramatic.

INVERSION ERROR

In order to evaluate the actual significance of the free surface effect for seismic exploration, AVO inversion using least squares was performed on models 1A-5A and 1B-5B by forward modeling. The fitted parameter for the inversion was the Poisson's ratio of the gas sand (σ_{gs}), since it is better constrained than density or velocity by the observed AVO relationship and typically is poorly known *a priori*. All other model parameters were assumed known, and so were held constant. Forward modeling for the vertical particle displacement amplitude at the free surface was first carried out using the true value for σ_{gs}. Following this, a series of seismic models were generated by sweeping through a broad range of σ_{gs}, calculating the total particle displacement amplitude of the emergent wave (A series) along with the vertical component of particle displacement for the emergent wave (B series) for each value of σ_{gs}, in order to simulate the exercise of attempting to match an observed AVO relationship without correctly compensating for the free surface effect. The RMS amplitude of each trace in a CMP gather was normalized by the RMS amplitude of the near offset trace, and the sum of the squared differences between the amplitude for each trial model trace and the corresponding reference trace was calculated. It was found empirically that an excellent fit could be obtained through the resulting data points using a least squares best fit polynomial of order three (Figure 6). The local minimum for each cubic equations was therefore taken as the best inversion estimate of σ_{gs} for each trial model.

The calculated values of σ_{gs} versus α_{ns} are plotted in Figure 7. In the cases where the total particle displacement of the emergent wavefield is used in forward modeling (models 1A-5A), the estimate of σ_{gs} is erroneously high. Conversely, when the vertical component of particle displacement for the emergent wavefield is used (models 1B-5B) the estimate of σ_{gs} is erroneously low. In both cases the magnitude of the inversion error grows with increasing near surface velocity. It is also evident that in areas where α_{ns} is low, the free surface effect can be neglected. The necessity to compensate for it will depend on the uncertainty tolerance for σ for a given exploration play.

DISCUSSION

Many active areas of exploration are covered with a sufficiently low velocity weathered layer to eliminate the need for free surface amplitude corrections prior to or during AVO inversion. However, the free surface effect is significant in areas where:

- bedrock is exposed;
- the ground is frozen to a significant depth.

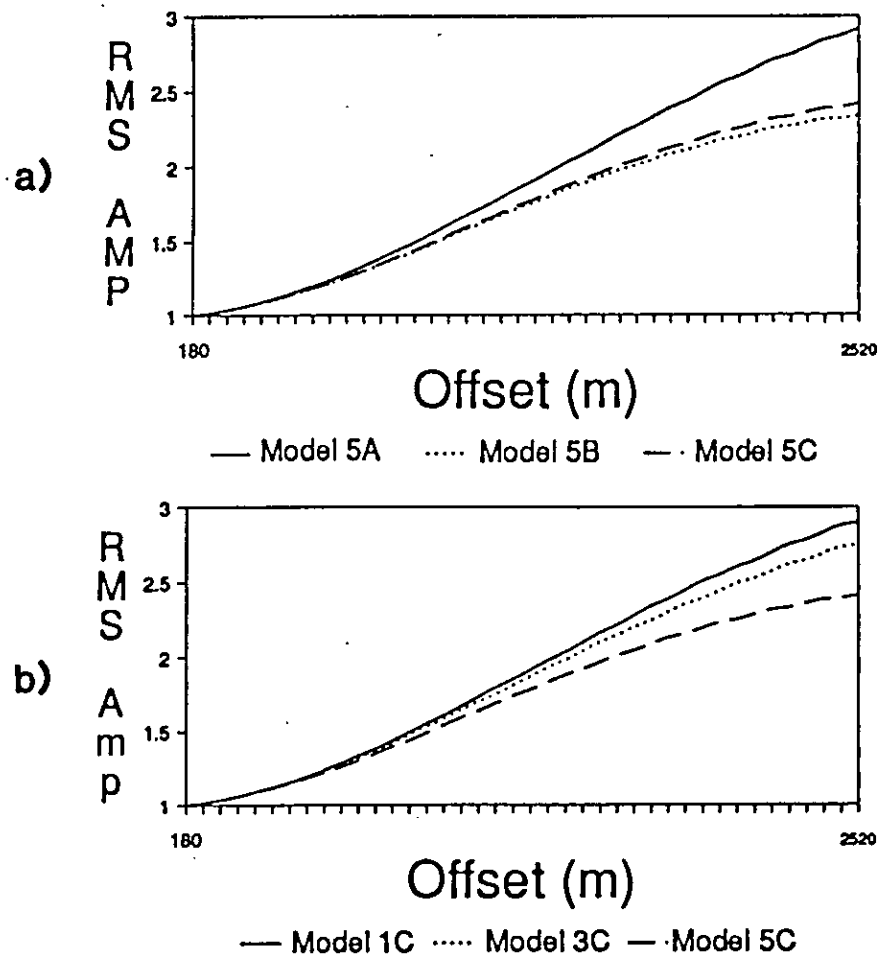

FIG. 5. (a) Plot of normalized RMS trace amplitude versus offset for models 5A-5C. The actual trace RMS amplitudes are normalized by the RMS amplitude of the near offset. (b) Plot of normalized RMS trace amplitude versus offset for models 1C-5C. The significance of the free surface effect increases with near surface velocity (increasing from 1C-5C).

The latter problem may be prevalent enough in northern areas for the free surface effect to be of concern in many situations. For example, shallow ice-bearing permafrost layers in the Canadian Arctic attain thicknesses of up to 70 m and are characterized by a P-wave velocity of ≈ 3500 m/s (Poley, 1987).

Correction for the free surface effect can be implemented in two ways; in the inverse sense by dynamic scaling of the observed seismic data, or in the forward sense by accounting for it in the inversion procedure. To accomplish the former, equation (2) can be rewritten in terms of the horizontal slowness p (Dankbaar, 1985, equation 1):

$$R_{\zeta}^{p}(p,\gamma_{ns},\beta_{ns}) = \frac{2\gamma_{ns}^{-1}(\gamma_{ns}^{2}-\beta_{ns}^{2}p^{2})^{1/2}(2\beta_{ns}^{2}p^{2}-1)}{(1-2\beta_{ns}^{2}p^{2})^{2} + 4p^{2}\beta_{ns}^{2}(\gamma_{ns}^{2}-\beta_{ns}^{2}p^{2})^{1/2}(1-\beta_{ns}^{2}p^{2})^{1/2}} \qquad (3)$$

Since R_{ζ}^{p} is real and non-singular for $p < \alpha^{-1}$, application of its inverse in the τ-p or f-k domain can be used to reverse the free surface effect. A technique similar to

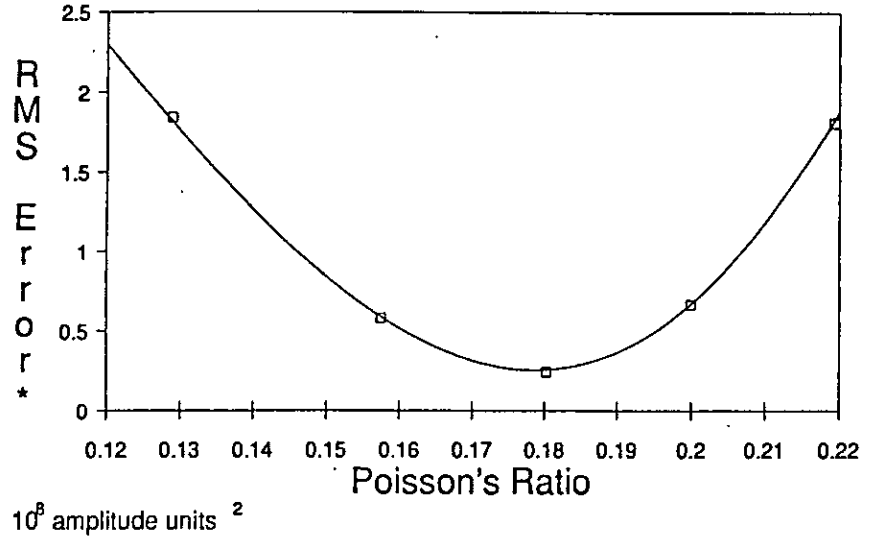

FIG. 6. Plot of sum of squared errors for inversion iterations for model 5A versus Poisson's ratio of the near surface layer. Solid line is best fit third order polynomial through data points. Minimum squared error occurs for σ_{ns} = 0.18, whereas actual value for σ_{ns} is 0.10.

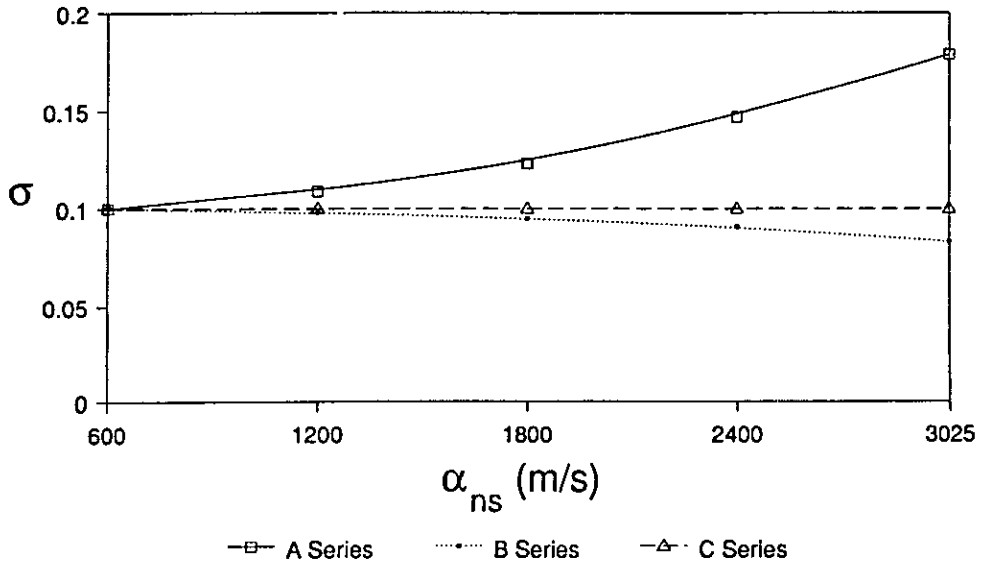

FIG. 7. Calculated estimated σ_{ns} versus near surface P-wave velocity for models 1A-5A and 1B-5B. The use of total particle displacement of the emergent ray in forward modeling causes the estimate of σ_{ns} to be erroneously high. Conversely, the use of the vertical component of particle displacement for the emergent ray causes the estimate of σ_{ns} to be erroneously low.

this that also performs wavefield separation on multicomponent records is discussed by Dankbaar (1985).

In many areas, the near surface weathered layer is very thin relative to the seismic wavelength within the bandwidth of the signal. In this case, the principals of assymptotic ray theory do not apply. Further research will be required to investigate the effect of a "thin skinned" near surface layer.

CONCLUSIONS

The amplitude and direction of particle displacement are altered by the interaction of an upgoing wavefield with the free surface. The magnitude of the free surface effect is primarily controlled by the angle of incidence at the free surface of the wavefield, which itself is governed by the P-wave velocity of the near surface layer. The effect of the free surface on the variation of amplitude with offset is most pronounced where the near surface P-wave velocity is high, such as on exposed bedrock or where the ground is deeply frozen. Failure to account for the free surface effect can lead to erroneous conclusions in the inversion of amplitude versus offset information. In the inversion example considered, failure to account for the free surface effect resulted in an error of up to 80% in the estimate of the Poisson's ratio of a gas sand.

ACKNOWLEDGMENTS

Funding for this research was provided by the Consortium for Research in Elastic Wave Exploration Seismology (the CREWES project) and by the Natural Sciences and Engineering Research Council. I would like to thank Dr. E. Krebes for his careful review of this manuscript and helpful suggestions.

REFERENCES

Aki, K. and Richards, P.G., 1980, Quantitative Seismology: Theory and Methods, W.H. Freeman and Company.

Dankbaar, J.W.M. 1985, Separation of P and S waves: Geophys. Prosp. **33**, 970-986.

Jain, S., 1987, Amplitude-offset analysis: A review with reference to application in Western Canada: J. Can. Soc. Expl. Geophys. **23**, 27-36.

Koefoed, O., 1955, On the effect of Poisson's ratios of rock strata on the reflection coefficients of plane waves: Geophys. Prosp. **3**, 381-387.

Moczo, P., Bard, P.V. and Psencik, J, 1987, Seismic response of two-dimensional absorbing structures by the ray method: J. Geophys., **62**, 38-49.

Ostrander. W.J., 1984, Plane-wave reflection coefficients for gas sands at nonnormal angles of incidence: Geophysics **49**, 1637-1648.

Poley, D.F., 1987, Acquisition and processing of high resolution reflection seismic data from permafrost affected areas of the Beaufort Sea continental shelf: Ph.D. thesis, Univ. of Calgary, Calgary, Alberta, 261 pp.

Rutherford, S.R. and Williams, R.H. 1989, Amplitude-versus-offset variations in gas sands:Geophysics, **54**, 680-688.

Young, B.C. and Braile, L.W., 1976, A computer program for the application of Zoeppritz's amplitude equations and Knott's energy equation: Bull. Seis. Soc. Am. **66**, 1881-1885.

Yu, G., 1985, Offset-amplitude variation and controlled-amplitude processing: Geophysics,**50**, 2697-2708.